Low pH Electrolytic Water Splitting Using Earth-Abundant Metastable Catalysts That Self-Assemble in Situ

Leanne G. Bloor, Pedro I. Molina, Mark D. Symes,* and Leroy Cronin*

WestCHEM, School of Chemistry, University of Glasgow, University Avenue, Glasgow G12 8QQ, U.K.

S Supporting Information

ABSTRACT: Typical catalysts for the electrolysis of water at low pH are based on precious metals (Pt for the cathode and IrO_2 or RuO_2 for the anode). However, these metals are rare and expensive, and hence lower cost and more abundant catalysts are needed if electrolytically produced hydrogen is to become more widely available. Herein, we show that electrode-film formation from aqueous solutions of first row transition metal ions at pH 1.6 can be induced under the action of an appropriate cell bias and that in the case of cobalt voltages across the cell in excess of 2 V lead to the formation of a pair of catalysts that show functional stability for oxygen evolution and proton reduction for over 24 h. We show that these films are metastable and that if the circuit is opened, they redissolve into the electrolyte bath with concomitant O_2 and H_2 evolution, such that the overall Faradaic efficiency for charge into the system versus amounts of gases obtained approaches unity for both O_2 and H_2. This work highlights the ability of first row transition metals to mediate heterogeneous electrolytic water splitting in acidic media by exploiting, rather than trying to avoid, the natural propensity of the catalysts to dissolve at the low pHs used. This in turn we hope will encourage others to examine the promise of metastable electrocatalysts based on abundant elements for a range of reactions for which they have traditionally been overlooked on account of their perceived instability under the prevailing conditions.
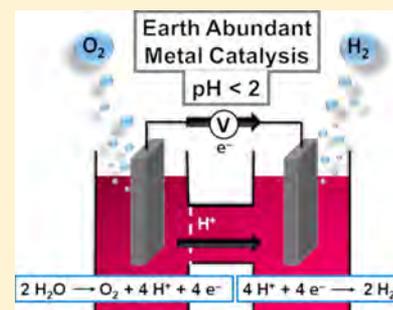
INTRODUCTION

The production of hydrogen via electrolytic water splitting is a process of considerable industrial importance and is one route by which sporadic renewable electrical power could be converted into storable fuel.[1−3] There currently exist several scientific and economic barriers to the adoption of electrolysis-driven water splitting as a viable fuel production route,[4] one of the most significant of which is the need to employ precious metal catalysts in low pH electrolyzers.[5] Replacement of these catalysts with more abundant first row transition metals is an attractive target, but the less noble character of these metals means that catalyst degradation and dissolution under the harsh operating conditions found in low pH water splitting devices could be problematic. If low pH water splitting using first row transition metals alone is to become a reality, then approaches that exploit and harness the tendency for these metals and their oxides to dissolve in acidic media must be developed.

In recent years, much attention has been focused on identifying heterogeneous first and second row transition metal electrocatalysts that can split water under neutral and near-neutral conditions.[6] Of the candidates identified, the most promising are those that possess the ability to self-assemble and regenerate (or "self-repair") in situ, such that catalysis can proceed in a continuous fashion at a steady rate. With regards to the anode reaction, Kanan and Nocera identified a self-repairing Co-oxide based catalyst that was effective for water oxidation at pHs above pH 5.[7,8] A nickel-based analogue was subsequently reported by the same group,[9] and in 2012 Zaharieva and Dau published details of a self-assembling water

oxidation electrocatalyst that uses manganese.[10] These water oxidation catalyst systems all operate in buffered solution at essentially neutral pH (pH 5−10), with anode film instability limiting water oxidation activity under more acidic conditions. Subsequent studies of the Nocera-type Co-oxide catalyst at lower pH values by Stahl and co-workers suggested that films for water oxidation could form and operate at pH 3.7 in fluoride-containing solutions,[11] but that at lower pHs (<3.5) water oxidation was mediated by homogeneous catalyst species without the formation of a heterogeneous catalyst film on the electrode.[12] The Co-oxide system has also been investigated as a precursor to a self-assembling proton reduction catalyst. Hence Cobo et al. were able to demonstrate that an electrodeposited Co-oxide film could not only act as a water oxidation catalyst but also could be converted into a Co-based proton reduction catalyst under reversal of the applied bias in phosphate buffer at pH 7.[13] Again, however, heterogeneous water splitting catalysis under strongly acidic conditions was not reported.

Several cathode materials that do operate under highly acidic conditions and yet do not rely on precious metals have been identified. The second-row transition metal molybdenum has a particularly rich chemistry in this regard, with MoS_2[14] (and related Mo_xS_y[15−17] compounds), MoB,[18] Mo_2C,[18,19] and nitrogen-doped Mo-Ni alloys[20] all showing high activity for sustained hydrogen evolution from acidic solutions. Interest-

ingly, Popczun et al. have recently added nickel phosphide (Ni_2P) to this list by noting parallels between the mode of action of MoS_2 and Ni_2P during catalytic hydrodesulfurization.[21] However, none of these low-pH hydrogen evolution catalysts display any obvious route for regeneration under their conditions of operation, and (save possibly for MoS_2 and its congeners) they tend to require several synthetic steps in order to yield the active catalyst.

In contrast, the first row transition metal oxide water oxidation catalysts previously mentioned all self-assemble from simple aqueous solutions of the relevant ions, and in the case of cobalt, dissolution and redeposition of the films has been linked to long-term functional stability.[22,23] Taken in combination with the work of Artero and co-workers,[13] this suggested to us that application of an appropriate bias across baths containing first row transition metal ions could lead to the simultaneous formation of catalysts for *both* the water oxidation and hydrogen evolution reactions. In particular, inspection of the Pourbaix diagram for cobalt (Figure 1) suggested that solid
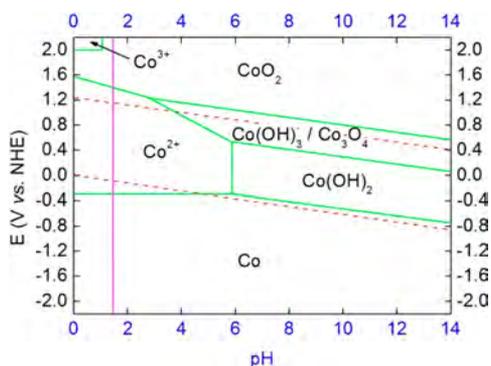
Figure 1. Simplified Pourbaix diagram for cobalt in aqueous solution. Green lines represent the borders of thermodynamic stability of the various species (adapted from ref 24). Dissolved species are considered as having an activity of 1. Red dashed lines mark the region of water stability, the lower line corresponding to the hydrogen evolution reaction and the upper line to the oxygen evolution reaction. The vertical magenta line is drawn at pH = 1.6 as a guide to the eye.

films of these species would be stable at pHs < 2, if bias potentials in excess of 2 V were applied across the electrolytic cell.[24] Hence we reasoned that Co-based films active for both the hydrogen and oxygen evolving half reactions could be deposited at low pH from the same electrolyte bath, provided that the concentration of Co(II) and the cell potential were sufficiently high. Lowering the cell bias below the threshold required to maintain stable Co and Co-oxide films would then lead to catalyst dissolution into the acidic medium as Co(II) species, providing a ready route to catalyst regeneration or removal if desired. In this way, the deposits would be metastable, constituting heterogeneous catalyst films only under the action of a suitably large bias.

Herein, we apply this approach to the deposition of films based on Co, Fe, Mn, and Ni at pH < 2 and show that when a potential difference of around 2 V is applied across a two-electrode electrolysis cell containing 0.2 M $Co_2(PO_4)_3$ at low pH (1.6), a pair of Co-based water splitting catalysts forms spontaneously and that these catalysts display functional stability for the oxygen and hydrogen evolving reactions for up to 30 h. Faradaic efficiencies for gas production during the electrolysis itself are around 60% for O_2 and 50% for H_2.

However, if the electrolysis is stopped and the circuit opened, the Co-based films redissolve into the acidic medium with noticeable bubbling, and upon complete dissolution of the films the Faradaic yield for both oxygen and hydrogen production approaches unity. Films based on the other metals considered either do not form or display noticeably poorer efficacy for the water splitting reactions. The reasons for these differences in behavior will be discussed, with reference to the relevant Pourbaix diagrams and in light of our experimental results.

RESULTS AND DISCUSSION

A typical experimental setup was as follows. Two indium tin oxide-coated (ITO) glass electrodes were connected in a two-electrode configuration in an electrolyte of Co(II) phosphate dissolved in 1 M H_3PO_4 to give a 0.6 M Co(II) solution and a final pH of 1.6. Both single-compartment and two-compartment cells (where the compartments were separated by a Nafion membrane) were used. In the case of cobalt, cell voltages in excess of 2.05 V (after correction for resistive losses; typically ~3 V before correction) led to the deposition of films on both electrodes, concomitant with bubbling. By comparison of the size of this potential window with the zones of stability indicated along the magenta line (pH = 1.6) in Figure 1, the deposition and persistence of these films is consistent with the simultaneous formation of Co metal on the cathode and a highly oxidized cobalt oxide on the anode (vide infra). Anode films tended to be black or dark brown, while cathode films were gray. Figure 2 shows a current versus time profile for a
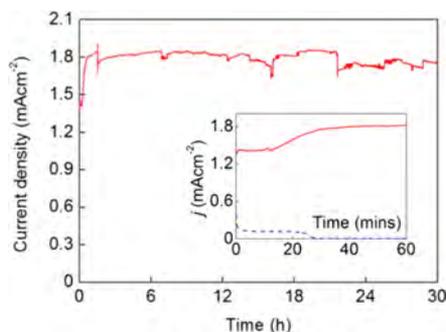
Figure 2. Bulk electrolysis of a 0.2 M solution of $Co_3(PO_4)_2$ in 1 M H_3PO_4 (final pH = 1.6) in a single chamber cell and a two-electrode configuration at room temperature. Both electrodes were ITO glass (7.5 cm^2) and the effective cell voltage corrected for resistive losses was 2.2 V (R = 61 Ω). Red line (main figure and inset): electrolysis in 0.2 M $Co_3(PO_4)_2$. Blue dashed line (inset only): electrolysis under the same conditions but in the absence of Co(II). All current densities are based on the geometrical surface area of the electrodes.

single compartment cell configuration in the presence and absence of 0.6 M Co(II) in 1 M H_3PO_4 at pH 1.6 and an effective voltage of 2.2 V. When Co(II) was present, a characteristic initial lag phase was observed as the catalysts deposited, followed by a rise in current and then a stable plateau due to catalytic water splitting (Figure 2 and inset, red line). This catalytic activity was then sustained over at least 30 h. Conversely, the current dropped off sharply after around 40 min in the absence of cobalt ions (Figure 2 inset, blue dashed line), and this was accompanied by a sharp rise in the resistance of the cathode and a change in its color. This in turn suggested that the cathodic deposit formed in 0.6 M Co(II) acted to protect the ITO cathode somewhat from reductive degrada-

tion.[25,26] The performance of this system at different applied voltages is given in the Supporting Information (Figure S2).

Cyclic voltammograms (CVs) on ITO in the presence of a 0.6 M Co(II) solution in a three-electrode configuration are shown in the Supporting Information, indicating that water oxidation onset occurs on the anode at between +1.4 and +1.5 V vs. NHE (Supplementary Figures S3 and S5), corresponding to about 0.3 V overpotential when high concentrations of Co(II) are present. Indeed, when bare ITO electrodes are poised at +1.5 V (vs Ag/AgCl) in solutions of 0.6 M Co(II) in 1 M H_3PO_4 at pH 1.6, brown films slowly develop on the anode with slow bubbling and current densities of around 0.4 mA cm^{-2} are achieved after 11 h (Supplementary Figure S4, all current densities are based on the geometrical surface area of the electrodes.). Electrolysis at +1.3 V vs Ag/AgCl did not produce any films, and current densities were comparable to those in the absence of Co(II). Proton reduction onset at the cathode in 0.2 M $Co_3(PO_4)_2$ at pH 1.6 is harder to gauge but appears to be between −0.4 and −0.6 V vs NHE (or about 0.3−0.5 V overpotential; Supplementary Figures S6 and S7). As suggested by CVs to reductive potentials at lower loadings of Co(II) (see Supplementary Figure S8), the large oxidative return wave at around −0.6 V vs Ag/AgCl in Supplementary Figure S6 could be due to stripping of deposited cobalt metal from the surface of the electrode.[27] Overall, these results imply a minimum cell voltage of around 2 V is necessary in order to split water to hydrogen and oxygen in 0.2 M $Co_3(PO_4)_2$ at pH 1.6, agreeing reasonably well with both the experimental observations and the Pourbaix diagram for Co shown in Figure 1.

In contrast to the stable operation shown in Figure 2 in 0.2 M $Co_3(PO_4)_2$ at pH 1.6, attempts to run the system in acidic media containing lower loadings of dissolved Co(II) met with only limited success. When a pair of catalysts were deposited for 1 h under conditions identical to those used in Figure 2 and then rinsed and immersed in a solution containing only 2 mM $Co_3(PO_4)_2$ in 1 M H_3PO_4 (adjusted to pH 1.6), current densities decayed to background levels within 2 h (Supplementary Figure S9). Inspection of the electrodes after this time revealed that the anode deposit had completely dissolved into the acidic medium (the cathode deposit had suffered less serious degradation). When anode films were polarized anodically in a three-electrode cell containing just 1 M H_3PO_4, current decay was even faster, with complete anode delamination occurring in under 4 min (see Supplementary Figure S10). Data showing how the current density for film deposition (and subsequent catalytic activity) varies with the varying concentration of $Co_3(PO_4)_2$ are shown in Supplementary Figure S11 for concentrations of 0.02, 0.2, 2, and 20 mM $Co_3(PO_4)_2$ in 1 M H_3PO_4 (adjusted to pH 1.6). These data show that at low concentrations (0.02 and 0.2 mM $Co_3(PO_4)_2$) the current densities after 12 h are similar to that of the control experiment (0 mM cobalt) and no film formation is observed. As the concentration of cobalt increases, a slight increase in current is observed (2 mM $Co_3(PO_4)_2$), although no films are evident on the electrodes after 11 h of electrolysis. At 20 mM $Co_3(PO_4)_2$, the current density stabilized around 0.4 mA cm^{-2} after 8 h. Thin deposits formed on both electrodes along with slow bubbling. Hence the presence of significant concentrations of Co(II) in the electrolyte bath seems essential for the maintenance of functional stability in this metastable catalyst pair, particularly with regard to the anode. This finding is in agreement with studies on the nucleation and growth of cobalt oxide-based water oxidation catalysts performed recently by Nocera and co-workers,[23] which suggest that nucleation of heterogeneous cobalt oxide water oxidation catalysts proceeds as the inverse third power in acid concentration, whereas the catalytic activity of these deposits scales as the inverse first order. This in turn implies that catalyst nucleation will only occur at low pHs (nucleation rate law dominating) if sufficiently high concentrations of Co(II) are present. Experimentally, we find that (at pH 1.6) the minimum concentration of Co(II) is somewhere between 2 and 20 mM.

We next investigated the effect of the counterion on catalytic performance. As both water oxidation and proton reduction are being probed simultaneously in this system, the supporting electrolyte anions must be stable to both highly oxidizing and highly reducing conditions. Phosphate is one such candidate, as are fluoride[11] and sulfate. Sulfate has previously been found to be a poor electrolyte for water oxidation with heterogeneous Co-oxides at neutral pH,[8,11] probably on account of the inability of SO_4^{2-} anions to accept protons at the pHs used in these previous reports (3.5 and above). However, the pK_a for the process $SO_4^{2-} + H^+ \rightarrow HSO_4^{2-}$ is 2, which is much closer to the pH used in this work (1.6), and hence we reasoned that sulfate might be able to mediate the necessary proton transfers required during water oxidation. Accordingly, we prepared a 0.6 M solution of $CoSO_4$ in water (adjusted to pH 1.6 with H_2SO_4) and used this as the electrolyte solution in a single-chamber, two-electrode configuration as before. This resulted in the formation of a pair of catalyst films very similar to those observed in cobalt phosphate baths, which were functionally stable for 24 h. The current density obtained with these films was at least as good as that obtained using $Co_2(PO_4)_3$ and also showed an intriguing oscillatory behavior over the first 16 h or so as the anode deposits grew, exfoliated, and regrew (see Supplementary Figure S12). At longer times ($t > 30$ h), the anode completely delaminated, and it was found that the underlying ITO electrode had ceased to be conductive. This long-term instability of the ITO coating on the anode was also a feature in $Co_2(PO_4)_3$ experiments and generally limited extended-time electrolysis experiments to less than 36 h. Thus we conclude that, at these concentrations of metal ions and at pH 1.6, sulfate is a suitable supporting electrolyte for sustained water splitting.

The effect of pH on the system was probed by adjusting the pH of 0.2 M $Co_2(PO_4)_3$ solutions with H_3PO_4 to give final pHs of 2.5, 2.0, 1.0, 0.5, and 0 (see Supplementary Figure S13). The results suggest that appreciable water splitting currents cannot be achieved at pH 1 and below. Inspection of the electrodes after 6 h of electrolysis revealed that deposits had formed on all cathodes, but that anode deposits did not form at pH ≤ 1. This suggests that anode stability is the limiting factor at low pH, an observation that agrees well with the bounds of stability for Co-oxide water oxidation catalysts suggested in the literature.[23]

Catalyst films deposited from phosphate electrolyte baths were analyzed using various techniques (XPS, EDX, SEM, elemental analysis, and powder X-ray diffraction of the anodic deposits). In the case of the anode, elemental analysis gave a Co:P ratio of 4:1, suggesting incorporation of phosphate within the electrode material. This theory was supported by XPS and EDX analyses (Supplementary Figures S14 and S15): XPS evinced binding energy peaks consistent with the presence of both a mixed Co(II)/Co(III) oxide (Co 2p peaks at 781 and 796 eV) and phosphate (P 2p peak at 133 eV),[28] while EDX

showed peaks for Co, P, and O in the bulk material. Overall, these data suggested that the isolated anode deposit had strong similarities to the "Co-Pi" catalyst reported by Nocera and co-workers at neutral pH.[7,29] Powder XRD of this material (Supplementary Figure S16) indicated that the material was highly amorphous, again in agreement with similar analysis performed by the Nocera group on their catalyst films.[7] Meanwhile, analysis of the cathodic deposits confirmed these to contain Co with only traces (∼0.2% by weight) of phosphorus, while EDX suggested the bulk structure to consist almost exclusively of cobalt metal (see Supplementary Figure S17). XPS analysis of the surface of the cathodic deposit (Supplementary Figure S18) showed that both phosphorus and oxygen were present alongside Co in a ratio of 2:2.6:8.5 (Co:P:O). This was in qualitative agreement with the cobalt hydrogen evolution catalyst formed at pH 7 that has been reported by Cobo et al.[13] SEM images of both anodic and cathodic deposits are given in Supplementary Figures S19 and S20.

The nature of the gases evolved during electrolysis was probed using gas chromatography headspace analysis (GCHA) in an airtight two-compartment electrolysis cell (see Supplementary Figure S1). Comparison of the amount of each gas produced with the total charge passed showed that the Faradaic yield for O$_2$ production *during electrolysis* was only slightly over 60% and that of H$_2$ was only 48%. As some of the charge passed during electrolysis must go toward catalyst formation, Faradaic efficiencies for O$_2$ and H$_2$ production of significantly less than 1 are not unexpected. Indeed, when cathode films were dried and weighed, >95% of the outstanding charge could be accounted for by assuming that these films consisted of Co metal (see Supporting Information, Section SI-4). However, when this method was applied to the oxide deposits on the anode, 30% of the charge passed during electrolysis was still unaccounted for.

At the pHs and potentials studied in this work, Pourbaix analysis and our own experimental results suggest that the cathode deposits should be Co metal,[24,30] while for the anode CoO$_2$ and/or Co$_3$O$_4$ are likely to be the dominant oxide phases.[24] In the absence of an applied bias, all of these species are unstable with respect to dissolution in pH 1.6 acid, according to the equations[31]

$$Co + 2H^+ \rightarrow Co^{2+} + H_2 \qquad (1)$$

$$2Co_3O_4 + 8H^+ \rightarrow 2CoO_2 + 4Co^{2+} + 4H_2O \qquad (2)$$

$$2CoO_2 + 4H^+ \rightarrow 2Co^{2+} + 2H_2O + O_2 \qquad (3)$$
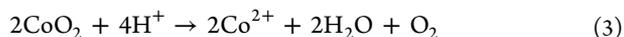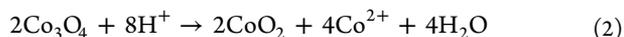
Hence we reasoned that Faradaic yields for the production of O$_2$ and H$_2$ from this system could approach unity if the cell headspace were analyzed after electrolysis had been terminated and as the films slowly dissolved. In support of this, both films were observed to bubble after electrolysis had ceased and the electrodes had been disconnected (see Supporting Information section SI-5 and Video SV1). Figure 3 shows how the percent of O$_2$ (Figure 3a) and H$_2$ (Figure 3b) in the cell headspace continued to rise for some hours after the termination of electrolysis, reaching a final Faradaic yield of 96% (±2%) for O$_2$ production and 92% (±4%) for H$_2$ production upon complete dissolution of the films. Likewise, Figure 4a and b show that film dissolution and simultaneous gas evolution after electrolysis has ceased is an effect that can be reproduced over multiple cycles. In the case of Figure 4a, the amount of
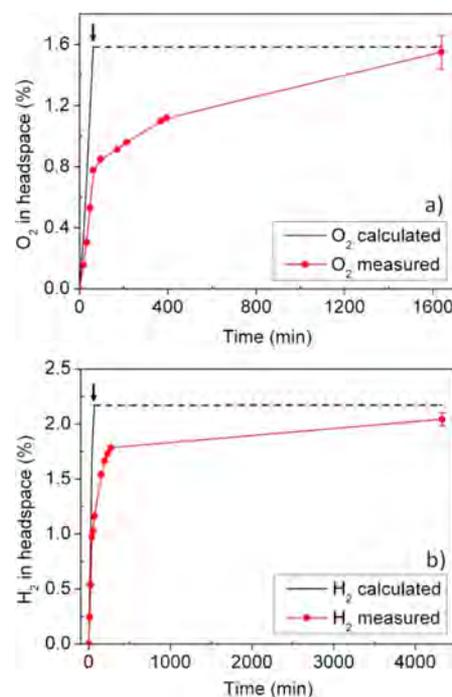
Figure 3. GCHA of airtight cells during and after electrolysis of a solution of 0.2 M Co$_3$(PO$_4$)$_2$ in 1 M H$_3$PO$_4$ at pH 1.6. Black solid lines indicate the % of a given gas expected in the cell headspace based on the charge passed during electrolysis (20 C was passed in both cases). Red circles indicate actual measurements of the percent of each gas in the cell headspace as deposited films slowly dissolved. Solid red lines and black dashed lines are provided as guides to the eye. Arrows indicates where electrolysis was stopped. (a) Oxygen evolution into the cell headspace. (b) Hydrogen evolution data.

oxygen in the cell headspace (red line and circles) is compared to the expected O$_2$ levels based on the amount of charge passed (black line) during periods when an effective voltage of around 2.2 V was applied across the cell (blue shading). Figure 4b gives analogous data for hydrogen production. In both cases, the volume % of gases in the headspace increased during periods when no electrolysis was occurring (as the films dissolved), although the timeframes were shorter than in Figure 3a and b and so the measured gas percentages did not have time to fully reach the expected levels.

After complete dissolution of the deposits, reapplication of the potential bias reconstituted the catalysts as before, with no apparent drop in subsequent catalytic activity (see Supplementary Figure S21). Hence Faradaic yields for gas production do indeed approach unity upon complete dissolution of the deposited metastable catalysts as part of a fully repeatable water splitting cycle. This in turn allows the efficiency of the cell to be determined (i.e., assuming that all of the current is used to produce hydrogen) by taking the ratio of the energy supplied to the cell versus the energy that would be released by the hydrogen that is produced, were it to be burnt in O$_2$. This gives an efficiency of 49% for the data shown in Figure 2 (with no *iR* drop correction) and 67% if the *iR* correction is taken into account (see Supporting Information for details).

Interestingly, the color of the pink-red Co(II) solution in the anode side of two-compartment cells was observed to darken significantly after extended periods of electrolysis. This color would fade within a few hours of the cessation of electrolysis, and the electrolyte would return to its original pink/red color.
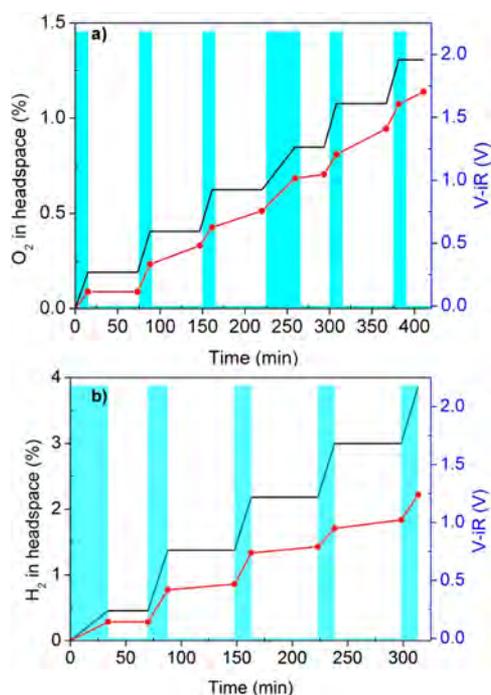
Figure 4. GCHA of airtight cells where electrolysis of a solution of 0.2 M $Co_3(PO_4)_2$ in 1 M H_3PO_4 at pH 1.6 has been stopped and restarted several times and the headspace of the cell sampled. Black solid lines (left-hand y-axis) indicate the % of oxygen or hydrogen expected in the cell headspace based on the charge passed during electrolysis. Red circles and red lines indicate actual measurements of the percent of oxygen or hydrogen in the cell headspace. The blue shaded areas (whose associated y-axis is on the right-hand side) indicate when an effective voltage of 2.2 V was applied and thus when electrolysis was occurring. (a) Oxygen evolution into the cell headspace, R = 129 Ω. (b) Hydrogen evolution data, R = 125 Ω.

Figure 5. TEM images of particles from the anode compartment of electrolysis cells containing 0.2 M $Co_3(PO_4)_2$ at pH 1.6. A two-electrode configuration was used, and both electrodes were ITO. The effective cell voltage was 2.4 V.

Electronic spectra of the darkened electrolyte immediately after electrolysis revealed a distinct absorption band at around 265 nm, but the visible region of the spectrum was changed very little from that of the pre-electrolysis solution. The band at 265 nm then completely disappeared as the solution returned to its initial pink/red color (see Supplementary Figure S22). Noting the absence of absorptions in the visible region of the spectrum that would account for the color change of the solution, we analyzed the anolyte for nanoparticulates using TEM.[32,33] This revealed the presence of nanoparticles of varying sizes (ranging from 10 nm to over 200 nm in diameter), where the larger particles appeared to be an agglomeration of smaller particles (see Figure 5).

If the dark anolyte solution was purged with Ar immediately after the cessation of electrolysis and this solution (without any electrodes) sealed in an airtight container, O_2 evolved spontaneously from the solution. When the amount of O_2 thus produced was compared to the charge passed during the electrolysis, this O_2 evolution from the anolyte was found to account for 30% of the total charge passed. Combined with the percentages of the charge already accounted for (~60% going to O_2 production during electrolysis and ~10% going to film formation as gauged by weighing, see above), it thus seems plausible that colloidal Co-oxide nanoparticles are forming during electrolysis of $Co_3(PO_4)_2$ solutions at pH 1.6 (either directly or by exfoliation from the anode) and are contributing to the water oxidation reaction, perhaps via eqs 2 and/or 3.[31] In this regard, we note that water oxidation at stabilized Co

nanoparticles (10−60 nm in diameter) has been reported recently by Shevchenko et al. at neutral pH.[34] However, the rate of O_2 evolution from our acidic anolyte suspensions is significantly slower than that of O_2 evolution *during* electrolysis (see Figure 3a).

Regarding the mechanism of water oxidation during electrolysis, we observed that if deposits from 0.2 M $Co_3(PO_4)_2$ on ITO glass were removed by gentle rubbing and the cleaned electrodes then returned to the 0.6 M Co(II) bath and subjected to the same conditions under which the films were originally grown, currents were initially very low and there was no bubbling evident. Films would, however, typically reform within 5−10 min at cell voltages in excess of 2.1 V and gas evolution would resume. This in turn implies that a significant fraction of the water splitting activity of the system comes about due to the heterogeneous deposits on the electrodes. Hence it appears that at least two mechanisms for water oxidation are occurring within the same system: heterogeneous water oxidation at the electrode surface during electrolysis and a slower heterogeneous water oxidation at colloidal Co-oxide particles. Indeed, homogeneous mechanisms such as those postulated by Gerken et al.[12] or Shafirovich and Strelets[35] could also be occurring in this system. The possibility of such a multireaction scenario in Co-oxide mediated water oxidation at near-neutral pH has recently been discussed in some detail by Stracke and Finke.[36]

The ease with which this pair of cobalt-based water splitting catalysts formed led us to consider which other first row transition metals might be amenable to the same kind of methods. Three attractive candidates were Mn, Fe, and Ni. In addition to the self-assembling Mn-oxide system mentioned earlier,[10] manganese oxides have also demonstrated activity for water oxidation under basic[37,38] and neutral/mildy acidic conditions,[39−42] and Mn-oxo cubanes are also found in the water splitting center of photosystem II in green plants.[43,44] Similarly, Fe-oxides have been shown to be active for water oxidation under photochemical conditions,[45,46] and mild steel has been employed as an electrode material for both the anode and cathode in alkaline electrolysis cells.[47] Nickel is also a popular choice for alkaline-regime anodes and cathodes,[47] and nickel oxides have shown utility for the water oxidation reaction at neutral pH.[9] Hence all three of these metals and/or their oxides are known to catalyze one or both of the half reactions of water splitting, albeit not under low pH conditions.

The Pourbaix diagram of manganese is shown in Figure 6. This suggests that at pH 1.6, cell voltages in excess of around
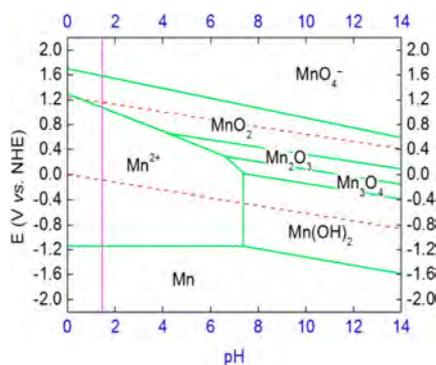
Figure 6. Simplified Pourbaix diagram for manganese in aqueous solution. Green lines represent the borders of thermodynamic stability of the various species (adapted from ref 24). Dissolved species are considered as having an activity of 1. Red dashed lines mark the region of water stability, the lower line corresponding to the hydrogen evolution reaction and the upper line to the oxygen evolution reaction. The vertical magenta line is drawn at pH = 1.6 as a guide to the eye.

2.2 V should be sufficient to drive the formation of deposits of Mn metal on the cathode and MnO_2 on the anode. Indeed, when a 0.5 M solution of $MnSO_4$ (pH adjusted to 1.6 with 0.5 M H_2SO_4) was subjected to electrolysis in a two-ITO electrode configuration as for cobalt (effective voltage = 2.8 V), a dark brown anode film and a grayish cathodic deposit were observed to form (see Supplementary Figures S23 and S24). Powder XRD of the anode film (Supplementary Figure S25) suggests a structure closely resembling ε-MnO_2 for this material.[48] After the first 2 h of electrolysis under these conditions, the current density was stable at around 0.3 mA cm^{-2} (see Supplementary Figure S26); however, this was only a tenth of that observed in the comparable cobalt system (Supplementary Figure S12), and gas production was correspondingly slower: a few bubbles were evident on the cathode and almost none at the anode. These slow kinetics relative to Co can be rationalized by examining the overpotentials required for the oxygen and hydrogen evolving half reactions in both cases. In acidic solutions, Kozin et al. found that Mn required an overpotential of 0.64 V at room temperature to achieve a current density of 1 mA cm^{-2} for hydrogen production.[49] Similarly, Mn-oxides have been variously reported to have overpotentials of 0.6 V at pH 5[10] and 0.9 V at pH 0[50,51] for a current density of 1 mA cm^{-2} for the oxygen evolution reaction. This suggests that minimum *iR*-corrected cell voltages somewhere between 2.7 and 2.8 V would need to be applied to generate 1 mA cm^{-2} in this low pH manganese system. In contrast, literature values for cobalt oxides suggest overpotentials of around 0.4 V are necessary for oxygen evolution at 1 mA cm^{-2} under neutral to mildly acidic conditions,[7] and overpotentials of around 0.4 V are required for hydrogen evolution at 1 mA cm^{-2} at very acidic pH (0.5–1 M H_2SO_4).[52,53] Thus for the cobalt system, current densities of 1 mA cm^{-2} could be expected at *iR*-corrected cell voltages exceeding 2.0–2.1 V. This last figure agrees reasonably well with our experimental data, despite the certain differences in reaction conditions probed. Hence it would seem that (although Mn and Mn-oxide deposits can form at these low pHs as predicted by the Pourbaix diagram) the greater overpotential requirements of the manganese system results in much lower current densities at the potentials investigated compared to Co(II) solutions at pH 1.6.

With regard to the cobalt system in the absence of Co(II) in the electrolyte, galvanostatic chronopotentiometry on films deposited from 0.2 M $Co_3(PO_4)_2$ in 1 M H_3PO_4 (pH adjusted to 1.6) indicated an initial overpotential requirement of ~0.46 V for the HER at 1 mA cm^{-2} (see Supplementary Figure S27). The Co loading for these cathode films was 0.8 mg cm^{-2}, equating to around 14 μmol Co per cm^2. This compares well with the loadings reported in ref 52 (20 mg cm^{-2}) for a similar overpotential requirement at low pH. Allied experiments with anode films (Supplementary Figure S28) indicated that to achieve a current density of 1 mA cm^{-2} for the OER an initial overpotential of around 0.9 V was required (anode loading of cobalt oxide was 0.8 mg cm^{-2}). However, determination of this overpotential was hampered by the instability of anode films in Co-free 1 M H_3PO_4 (dissolution seemed complete within 60 s), which probably leads to a large overestimation of the potential required to achieve this current density. Indeed, Stahl and co-workers report 0.4 V overpotential to reach this current density with thin Co-oxide films (30–60 mC cm^{-2}) at pH 3.4 where film dissolution is less problematical.[12] In terms of other first row transition metal catalysts for the OER, Mn-oxides have been shown to operate at 1 mA cm^{-2} under the following conditions: 0.9 V overpotential at pH 0 (loading = 10 μmol Mn per cm^2),[50] 590 mV overpotential at pH 7 (loading = 5.4 μg cm^{-2}),[10] and around 0.3 V overpotential at pH 13 (loading = 28 μg cm^{-2}).[37]

To examine whether nickel would act in a similar way to cobalt, a 0.5 M solution of $NiSO_4$ (adjusted to pH 1.6 with 0.5 M H_2SO_4) was examined in a two-ITO electrode configuration with an effective voltage of 2.9 V. The Pourbaix diagram for nickel (see Supplementary Figure S29)[24] suggests that this potential should be sufficient to facilitate the deposition of Ni on the cathode, but the nature of any anodic deposit is less easy to predict on the basis of the Pourbaix diagram alone. For example, there is some uncertainty as to what oxides of Ni exist under acidic conditions,[54] with structural studies suggesting that nickel oxide films do not form at potentials higher than +1.7 V (vs NHE) at low pH.[55] This was borne out by our own results: metallic films of Ni(0) were deposited on the cathode (see Supplementary Figure S30), but no film formation was evident on the anode. Current densities were generally poor, not exceeding 0.2 mA cm^{-2} until at about 40 min a dramatic decrease in current was observed, concomitant with a sharp increase in the resistance of the ITO coating on the electrodes (see Supplementary Figure S31). Again, only a very small number of bubbles collected on the cathode over the course of the experiment, and there was no obvious bubbling at the anode. These data are consistent with the formation of a metallic nickel film and a small amount of hydrogen production at the cathode (either by dissolution of the Ni(0) into the acidic medium or by heterogeneous catalysis at the Ni film), but otherwise appreciable overall water splitting was not observed.

Finally, we examined electrolysis of 0.5 M solutions of $FeSO_4$ (adjusted to pH 1.6 with 0.5 M H_2SO_4) at effective voltages of 2.1 V. As with Ni, Pourbaix analysis (see Supplementary Figure S32) supports the supposition that a metallic Fe cathode deposit will form, but the nature of the anodic Fe species is less clear.[56] In the event, we did indeed observe that metallic Fe deposited onto the cathode (see EDX spectrum in Supplementary Figure S33), but no deposits were seen at the anode. Current densities were comparatively high (generally in excess of 1.5 mA cm^{-2} over 10 h, Supplementary Figure S34), but no

bubbling was observed at the anode that would be consistent with water splitting. Instead, it seems likely that the dominant anode reaction is oxidation of Fe(II) to Fe(III) species as suggested by the Pourbaix diagram.

CONCLUSIONS

In summary, we have presented a rational route to identifying candidates for low pH water splitting using non-noble metals and have demonstrated the utility of this approach by characterizing a pair of self-assembling and functionally stable catalysts for electrolytic water splitting at low pH based on cobalt. The catalysts themselves are metastable, displaying activity for water splitting for over 24 h, but redissolving into the acidic medium (with continued gas evolution) in the absence of an applied bias. Hence these metastable films act to some extent as short-term buffers of electrolytic gas production, allowing continued gas evolution during periods when no bias is applied across the cell. In the event of complete catalyst dissolution during longer periods without bias, catalyst films can be reconstituted from the medium by reapplication of an appropriate potential.

The mechanism of action is interesting for several reasons. First, heterogeneous films form and mediate water splitting at pHs well below those at which the catalysts dissolve when there is no voltage across the cell. Second, nanoparticles appear in the anode-compartment solutions, and these continue to mediate water oxidation after the potential and electrodes have been removed from solution, demonstrating that two separate heterogeneous water oxidation reaction mechanisms are occurring. Third, we note that gas evolution continues from the deposited films themselves long after electrolysis has ceased and the electrodes have been electrically disconnected, as the films redissolve into the acidic medium. This results in visible and sustained bubbling from both electrodes for several minutes after the circuit has been broken. In this way, we were able to demonstrate essentially full Faradaic efficiency for both oxygen and hydrogen evolution in this system. To the best of our knowledge, this is the first time that a complete water splitting cycle has been reported at such low pH using only first row transition metals. Moreover, the system is able to cycle and produce gas at full Faradaic efficiency precisely because both catalysts are inherently unstable with respect to dissolution at the pHs probed.

Transition metal ions can lead to the degradation of Nafion membranes through Fenton-type reactions, whereby hydrogen peroxide is decomposed to radical oxygen species (ROS) which then attack the Nafion polymer backbone.[57,58] This is a common cause of degradation in all electrolyzers that use Nafion. In this regard, recent work by Ramani and co-workers shows that incorporation of CeO_2 into Nafion membranes can significantly mitigate ROS-induced damage of Nafion membranes, by cycling between Ce(IV) and Ce(III).[59,60] Importantly, the active cerium(IV) oxide radical scavenger can then be regenerated in acidic media, providing a potential route to protecting Nafion from ROS.[61]

Finally, we note the relative success of using Pourbaix diagrams to predict which metal ion solutions will form heterogeneous deposits (and on which electrodes) under the application of a bias in a two-electrode configuration. In combination with recent efforts by Bard and co-workers to introduce kinetic data into E vs pH charts,[62] we predict that the approach outlined in this work will generate an increasingly sophisticated library of metastable first row transition metal electrocatalysts for a range of transformations.

EXPERIMENTAL SECTION

Two- and three-electrode electrochemical studies were performed using a CH Instruments CHI760D potentiostat at room temperature (20 °C). Two-electrode studies were performed by attaching the counter and reference leads to the same electrode, thus giving a floating reference configuration. In the three-electrode configuration, a Pt mesh counter electrode was used, along with an Ag/AgCl (NaCl, 3 M) reference electrode (RE 5B, BASi). Electrodes were washed with acetone and deionized water prior to use. Three-electrode potentials were converted to the NHE reference scale using $E(\mathrm{NHE}) = E(\mathrm{Ag}/\mathrm{AgCl}) + 0.209$ V.

Bulk electrolyses were performed in a two-electrode configuration in both single-compartment and two-compartment electrochemical cells. In the latter case, the compartments of the H-cell were separated by a 0.180 mm-thick Nafion N-118 membrane, with this membrane being held in place by judicious application of Araldite epoxy glue (Bostik Findley, Ltd., U.K.). In a typical experiment, both compartments of the H-cell contained 80 mL of 0.2 M $Co_3(PO_4)_2$ in 1 M H_3PO_4. Both electrodes were 2.5 cm × 7.5 cm pieces of ITO-coated glass rinsed with acetone and deionized water prior to use. Typically, an area of 7.5 cm^2 of these electrodes was taped off with sticky tape and exposed to the $Co_3(PO_4)_2$ solution, and uncorrected voltages of 3 V (between 2.1 and 2.4 V after correction for solution resistance) were applied across the cell. Solutions were not stirred. In single compartment configurations the procedure was similar, with the exception that both electrodes were held in place in the single compartment cell at a distance of 1.5 cm from each other in a 25 mL beaker. Voltages were corrected for the ohmic resistance of the cells to give an effective voltage ($V_{\mathrm{effective}}$) according to the formula:[63]

$$V_{\mathrm{effective}} = V_{\mathrm{applied}} - iR \tag{4}$$

where i is the current flowing through the cell and R is the resistance of the cell. Cell resistances were measured by the iR test function available on the potentiostats, by the general method developed by He and Faulkner (see Supporting Information for details).[64] The error associated with this iR-correction is dominated by the error associated with gauging the resistance of the solution, where values were found to vary over a range of $R_{\mathrm{measured}} \pm 3\%$.

ASSOCIATED CONTENT

Ⓢ Supporting Information

Experimental protocols, additional electrochemical data, details of gas analysis, structural and spectroscopic characterization of deposits, simplified Pourbaix diagrams for Ni and Fe, and video file. This material is available free of charge via the Internet at http://pubs.acs.org.

AUTHOR INFORMATION

Corresponding Authors
mark.symes@glasgow.ac.uk
lee.cronin@glasgow.ac.uk

Notes

The authors declare no competing financial interest.

■ REFERENCES

(1) Cook, T. R.; Dogutan, D. K.; Reece, S. Y.; Surendranath, Y.; Teets, T. S.; Nocera, D. G. *Chem. Rev.* **2010**, *110*, 6474.

(2) Olah, G. A.; Prakash, G. K. S.; Goeppert, A. *J. Am. Chem. Soc.* **2011**, *133*, 12881.

(3) Armaroli, N.; Balzani, V. *ChemSusChem* **2011**, *4*, 21.

(4) Holladay, J. D.; Hu, J.; King, D. L.; Wang, Y. *Catal. Today* **2009**, *139*, 244.

(5) Carmo, M.; Fritz, D. L.; Mergel, J.; Stolten, D. *Int. J. Hydrogen Energ.* **2013**, *38*, 4901.

(6) Symes, M. D.; Cronin, L. In *Materials for a Sustainable Future*; Letcher, T. M., Scott, J. L., Eds.; Royal Society of Chemistry: London, 2012.

(7) Kanan, M. W.; Nocera, D. G. *Science* **2008**, *321*, 1072.

(8) Lutterman, D. A.; Surendranath, Y.; Nocera, D. G. *J. Am. Chem. Soc.* **2009**, *131*, 3838.

(9) Dincă, M.; Surendranath, Y.; Nocera, D. G. *Proc. Natl. Acad. Sci. U.S.A.* **2010**, *107*, 10337.

(10) Zaharieva, I.; Chernev, P.; Risch, M.; Klingan, K.; Kohlhoff, M.; Fischer, A.; Dau, H. *Energy Environ. Sci.* **2012**, *5*, 7081.

(11) Gerken, J. B.; Landis, E. C.; Hamers, R. J.; Stahl, S. S. *ChemSusChem* **2010**, *3*, 1176.

(12) Gerken, J. B.; McAlpin, J. G.; Chen, J. Y. C.; Rigsby, M. L.; Casey, W. H.; Britt, R. D.; Stahl, S. S. *J. Am. Chem. Soc.* **2011**, *133*, 14431.

(13) Cobo, S.; Heidkamp, J.; Jacques, P.-A.; Fize, J.; Fourmond, V.; Guetaz, L.; Jousselme, B.; Ivanova, V.; Dau, H.; Palacin, S.; Fontecave, M.; Artero, V. *Nat. Mater.* **2012**, *11*, 802.

(14) Hinnemann, B.; Moses, P. G.; Bonde, J.; Jørgensen, K. P.; Nielsen, J. H.; Horsh, S.; Chorkendorff, I.; Nørskov, J. K. *J. Am. Chem. Soc.* **2005**, *127*, 5308.

(15) Hou, Y.; Abrams, B. L.; Vesborg, P. C. K.; Björketun, M. E.; Herbst, K.; Bech, L.; Setti, A. M.; Damsgaard, C. D.; Pedersen, T.; Hansen, O.; Rossmeisl, J.; Dahl, S.; Nørskov, J. K.; Chorkendorff, I. *Nat. Mater.* **2011**, *10*, 434.

(16) Merki, D.; Fierro, S.; Vrubel, H.; Hu, X. *Chem. Sci.* **2011**, *2*, 1262.

(17) Merki, D.; Hu, X. *Energy Environ. Sci.* **2011**, *4*, 3878.

(18) Vrubel, H.; Hu, X. *Angew. Chem., Int. Ed.* **2012**, *51*, 12703.

(19) Chen, W.-F.; Wang, C.-H.; Sasaki, K.; Marinkovic, N.; Xu, W.; Muckerman, J. T.; Zhu, Y.; Adzic, R. R. *Energy Environ. Sci.* **2013**, *6*, 943.

(20) Chen, W.-F.; Sasaki, K.; Ma, C.; Frenkel, A. I.; Marinkovic, N.; Muckerman, J. T.; Zhu, Y.; Adzic, R. R. *Angew. Chem., Int. Ed.* **2012**, *51*, 6131.

(21) Popczun, E. J.; McKone, J. R.; Read, C. G.; Biacchi, A. J.; Wiltrout, A. M.; Lewis, N. S.; Schaak, R. E. *J. Am. Chem. Soc.* **2013**, *135*, 9267.

(22) Bediako, D. K.; Lassalle-Kaiser, B.; Surendranath, Y.; Yano, J.; Yachandra, V. K.; Nocera, D. G. *J. Am. Chem. Soc.* **2012**, *134*, 6801.

(23) Surendranath, Y.; Lutterman, D. A.; Liu, Y.; Nocera, D. G. *J. Am. Chem. Soc.* **2012**, *134*, 6326.

(24) Pourbaix, M. In *Atlas of Electrochemical Equilibria in Aqueous Solutions*; Franklin, J. A., Trans.; National Association of Corrosion Engineers: Houston, TX, 1974.

(25) Monk, P. M. S.; Man, C. M. *J. Mater. Sci.: Mater. Electron.* **1999**, *10*, 101.

(26) Senthilkumar, M.; Mathiyarasu, J.; Joseph, J.; Phani, K. L. N.; Yegnaraman, V. *Mater. Chem. Phys.* **2008**, *108*, 403.

(27) Vanýsek, P. In *Handbook of Chemistry and Physics*, 93rd ed.; Haynes, W. M., Ed.; CRC Press: Boca Raton, 2012.

(28) Moulder, J. F.; Stickle, W. F.; Sobol, P. E.; Bomben, K. D. In *Handbook of X-ray Photoelectron Spectroscopy*; Perkin-Elmer: Eden Prairie, MN, 1992.

(29) Surendranath, Y.; Dincă, M.; Nocera, D. G. *J. Am. Chem. Soc.* **2009**, *131*, 2615.

(30) Chivot, J.; Mendoza, L.; Mansour, C.; Pauporté, T.; Cassir, M. *Corros. Sci.* **2008**, *50*, 62.

(31) Da Silva, L. M.; Boodts, J. F. C.; De Faria, L. A. *Electrochim. Acta* **2001**, *46*, 1369.

(32) Haiss, W.; Thanh, N. T. K.; Aveyard, J.; Fernig, D. G. *Anal. Chem.* **2007**, *79*, 4215.

(33) Bohren, C. F.; Huffman, D. R. In *Absorption and Scattering of Light by Small Particles*; Wiley-Interscience: New York, 1983.

(34) Shevchenko, D.; Anderlund, M. F.; Thapper, A.; Styring, S. *Energy Environ. Sci.* **2011**, *4*, 1284.

(35) Shafirovich, V. Y.; Strelets, V. V. *Nouv. J. Chim.* **1978**, *2*, 199.

(36) Stracke, J. J.; Finke, R. G. *ACS Catal.* **2013**, *3*, 1209.

(37) Gorlin, Y.; Jaramillo, T. F. *J. Am. Chem. Soc.* **2010**, *132*, 13612.

(38) Takashima, T.; Hashimoto, K.; Nakamura, R. *J. Am. Chem. Soc.* **2012**, *134*, 1519.

(39) Harriman, A.; Pickering, I. J.; Thomas, J. M.; Christensen, P. A. *J. Chem. Soc., Faraday Trans. 1* **1988**, *84*, 2795.

(40) Jiao, F.; Frei, H. *Chem. Commun.* **2010**, *46*, 2920.

(41) Najafpour, M. N.; Ehrenberg, T.; Wiechen, M.; Kurz, P. *Angew. Chem., Int. Ed.* **2010**, *49*, 2233.

(42) Hocking, R. K.; Brimblecombe, R.; Chang, L.-Y.; Singh, A.; Cheah, M. H.; Glover, C.; Casey, W. H.; Spiccia, L. *Nat. Chem.* **2011**, *3*, 461.

(43) Barber, J. *Inorg. Chem.* **2008**, *47*, 1700.

(44) Umena, Y.; Kawakami, K.; Shen, J. R.; Kamiya, N. *Nature* **2011**, *473*, 55.

(45) Hardee, K. L.; Bard, A. J. *J. Electrochem. Soc.* **1976**, *123*, 1024.

(46) Tilley, S. D.; Cornuz, M.; Sivula, K.; Grätzel, M. *Angew. Chem., Int. Ed.* **2010**, *49*, 6405.

(47) Zeng, K.; Zhang, D. *Prog. Energ. Combust.* **2010**, *36*, 307.

(48) Kim, C.-H.; Akase, Z.; Zhang, L.; Heuer, A. H.; Newman, A. E.; Hughes, P. J. *J. Solid State Chem.* **2006**, *179*, 753.

(49) Kozin, L. F.; Mashkova, N. V.; Manilevich, F. D. *Prot. Met. Phys. Chem. Surf.* **2009**, *45*, 25.

(50) Morita, M.; Iwakura, C.; Tamura, H. *Electrochim. Acta* **1977**, *22*, 325.

(51) Jiao, F.; Frei, H. *Energy Environ. Sci.* **2010**, *3*, 1018.

(52) Rojas, M.; Fan, C. L.; Miao, H. J.; Piron, D. L. *J. Appl. Electrochem.* **1992**, *22*, 1135.

(53) Povroznik, V. S.; Shein, A. B. *Prot. Met.* **2007**, *43*, 203.

(54) Beverskog, B.; Puigdomenech, I. *Corros. Sci.* **1997**, *39*, 969.

(55) Hoppe, H.-W.; Strehblow, H.-H. *Corros. Sci.* **1990**, *31*, 167.

(56) Beverskog, B.; Puigdomenech, I. *Corros. Sci.* **1996**, *38*, 2121.

(57) Curtin, D. E.; Lousenberg, R. D.; Henry, T. J.; Tangeman, P. C.; Tisack, M. E. *J. Power Sources* **2004**, *131*, 41.

(58) Chen, C.; Levitin, G.; Hess, D. W.; Fuller, T. F. *J. Power Sources* **2007**, *169*, 288.

(59) Trogadas, P.; Parrondo, J.; Ramani, V. *Electrochem. Solid St.* **2008**, *11*, B113.

(60) Prabhakaran, V.; Arges, C. G.; Ramani, V. *Proc. Natl. Acad. Sci. U.S.A.* **2012**, *109*, 1029.

(61) Czapski, G.; Bielski, B. H. J.; Sutin, N. *J. Phys. Chem.* **1963**, *67*, 201.

(62) Minguzzi, A.; Fan, F.-R. F.; Vertova, A.; Rondinini, S.; Bard, A. J. *Chem. Sci.* **2012**, *3*, 217.

(63) Hamann, C. H.; Hamnett, A.; Vielstich, W. *Electrochemistry*, 2nd ed.; Wiley-VCH: Weinheim, 2007.

(64) He, P.; Faulkner, L. R. *Anal. Chem.* **1986**, *58*, 517.